Supporting Information

Mesoporous Cobalt Difluoride Synchronizes Aluminum Oxidation and Perchlorate Decomposition for Enhanced Oxygen Transfer in Energetic Composites

Authors:

✦ ***Yuxiang Li*** [1,2]* *orcid.org/0000-0002-1172-9329* *Email*: liyx_ich@hotmail.com*

✦ ***Kaili Zhang*** [1,2]* *orcid.org/0000-0002-5926-2019* *Email*: kaizhang@cityu.edu.hk*

[1] *Department of Mechanical Engineering, City University of Hong Kong, 83 Tat Chee Avenue, Hong Kong SAR, China.*

[2] *Hong Kong Branch of National Precious Metals Material Engineering Research Centre, 83 Tat Chee Avenue, Hong Kong SAR, China.*

Table of content

● Sample preparation

SAFETY CAUTION! Energetic composites containing Al powder are flammable and explosive substances, which must be handled with extreme care and apply standard safety precautions (e.g., spark-free tools, static control, and appropriate personal protective equipment). In addition, as fluorides exhibit strong corrosion toward silicate-based materials, common glassware should not be used for their handling, storage, or reaction processes. In addition, due to the high toxicity of fluorides, waste solutions and off-gases containing fluorides require specialized treatment, such as neutralization with concentrated calcium chloride solution to precipitate insoluble CaF_2. We recommend preparing calcium gluconate gel in laboratory first-aid kits to treat accidental skin exposure to fluorides.

Raw chemicals for synthesis, including cobalt nitrate hexahydrate ($Co(NO_3)_2{\cdot}6H_2O$), ammonium hydrogen bifluoride (NH_4HF_2), sodium perchlorate ($NaClO_4$), and potassium bromide (KBr), were purchased from Shanghai Aladdin Reagent Co. Ltd with AR-grade purity. ACS-grade absolute ethanol and isopropyl alcohol were sourced from Hong Kong Anaqua Co. Ltd. Deionized water was produced from a Milli-Q purification system (water resistivity of 18 MΩ·cm). All chemicals and solvents were used as received without further purification.

○ Note S1. Synthesis of NH_4CoF_3 precursor

The ammonium cobalt trifluoride (NH_4CoF_3) precursor was synthesized via a solvothermal reaction. Generally, 5.24 g (18 mmol) of $Co(NO_3)_2{\cdot}6H_2O$ was dissolved in 50 mL of absolute ethanol in a Teflon beaker. Subsequently, 10 mL of pre-prepared aqueous solution of NH_4HF_2 (7.2 mol/L) was added dropwise to the ethanolic solution of $Co(NO_3)_2$ under magnetic stirring, forming a pale pink suspension. The suspension was transferred to a 100mL Teflon-lined stainless-steel autoclave and heated in an electric oven at 120 °C for 10 h (heating rate: 1 °C/min). After cooling naturally to room temperature, the **deep purple** precipitate at the bottom was centrifuged and washed three times with absolute ethanol, followed by drying in a vacuum oven at 70 °C for 2 h. The proposed reaction formula is given as follows:

$$[Co(H_2O)_6](NO_3)_2 + 3NH_4HF_2 \xrightarrow{EtOH/H_2O\_120\,℃} NH_4CoF_3\downarrow + 2NH_4NO_3 + 6H_2O + 3HF$$

Nevertheless, excessive NH_4HF_2 was used to ensure the completion of reaction, which is indicated by the transparent and colorless supernatant (no red color $[Co(H_2O)_6]^{2+}$ ions). Because NH_4CoF_3 is soluble in water yet nearly insoluble in ethanol, washing the precipitate with ethanol instead of water can prevent the loss of the product.

Notably, the morphology of NH_4CoF_3 is significantly influenced by the solvent environment (ethanol/water ratio) and the NH_4HF_2/$Co(NO_3)_2$ molar ratio (**Table S1**, **Figure S1**), demonstrating the tunability of this synthesis method and its potential for creating tailored microstructures [1, 2]. Additionally, NH_4CoF_3 remains stable at room temperature under dry conditions, as evidenced by unchanged XRD patterns of powder stored in airtight containers for over three years compared to freshly synthesized sample.

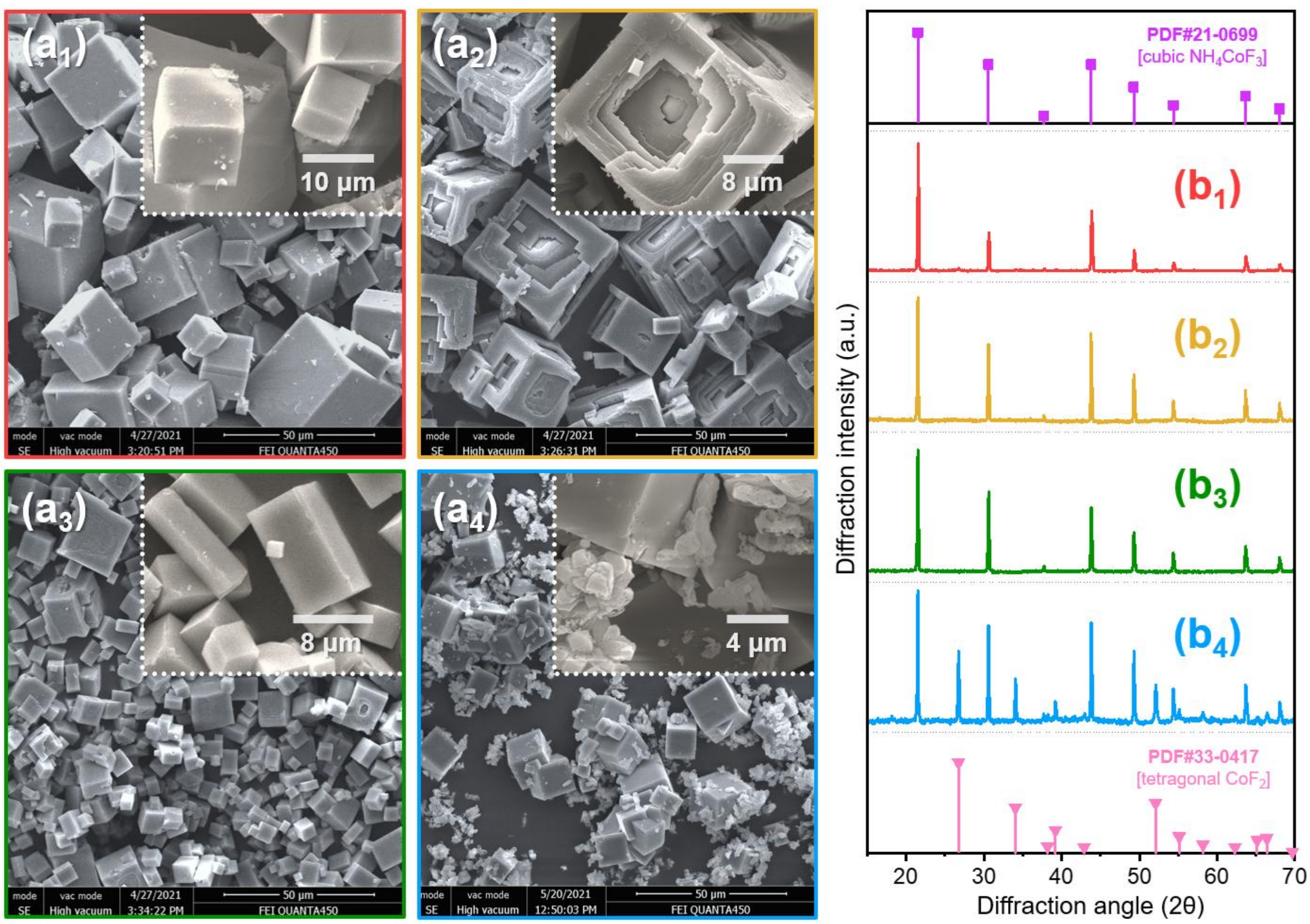

Figure S1. (**a**) *SEM images and* (**b**) *XRD patterns of sample synthesized at different conditions. The subscript 1–4 corresponds to Sample 1–4 in Table S1.*

Table S1. *Synthesis of NH_4CoF_3 at different conditions. All samples were produced from hydrothermal reaction at 120 °C for 10 h.*

Label	$Co(NO_3)_2·6H_2O$ [mmol]	EtOH [mL]	NH_4HF_2 [mmol]	H_2O [mL]
Sample 1	18	50	48	10

Sample 2	18	50	96	10
Sample 3	18	40	72	20
Sample 4	18	50	24	10

○ Note S2. Synthesis of porous CoF_2 and Co_3O_4

The preparations of CoF_2 and Co_3O_4 are based on the following reactions:

$$NH_4CoF_3 \xrightarrow{250\sim350\ ℃} CoF_2 + NH_3 \uparrow + HF \uparrow$$

$$CoF_2 + H_2O + \frac{1}{6}O_2 \xrightarrow{>500\ ℃} \frac{1}{3}Co_3O_4 + 2HF$$

The mesoporous CoF_2 (p-CoF_2) was prepared through calcination of NH_4CoF_3 precursor (loaded in an alumina boat) in an alumina tube furnace under argon atmosphere at 350 °C for 2 h (heating rate: 2 °C/min). Although this conversion is based on the intramolecular decomposition of NH_4CoF_3, an inert atmosphere (argon or nitrogen) can prevent degradation from ambient air (e.g., hydrolysis or oxidation). The obtained p-CoF_2 sample is a **pale pink** powder.

On the other hand, porous Co_3O_4 (p-Co_3O_4) was prepared through calcination of NH_4CoF_3 precursor (or aforementioned p-CoF_2) in an alumina tube furnace under air atmosphere at 750 °C for 4 h (heating rate: 2 °C/min). Notably, the pyrohydrolysis of CoF_2 to Co_3O_4 is a gas-solid reaction where water vapor is an indispensable reactant. Therefore, increasing the humidity via controlled steam introduction (or inversely, reducing solid load) can facilitate the conversion at relatively low temperature (though still above 500 °C) and shorten the reaction duration. The obtained p-Co_3O_4 sample is a shiny **black** powder. The distinct color change can serve as a preliminary visual indicator of complete conversion.

○ Note S3. Synthesis of $KClO_4$

Potassium perchlorate ($KClO_4$) was prepared via a conventional precipitation method as follows:

$$NaClO_4 + KBr \longrightarrow KClO_4 \downarrow + NaBr$$

Briefly, 100 mL of $NaClO_4$ aqueous solution (1 mol/L) was added dropwise into 100 mL of KBr aqueous solution (1 mol/L) under continuous magnetic stirring at room temperature (~25 °C) for 1 h. The resulting white precipitate was isolated by centrifugation and washed three times with deionized water to remove residual ions (Na^+, Br^-). The crude $KClO_4$ precipitate was pulverized using a QM-3SP04 planetary ball mill machine (NJU-Instrument Ltd.) at ambient temperature for 24 h. Absolute ethanol served as the dispersing medium to minimize particle agglomeration during milling. The characterizations of the milled $KClO_4$ are shown in **Figure S2**.

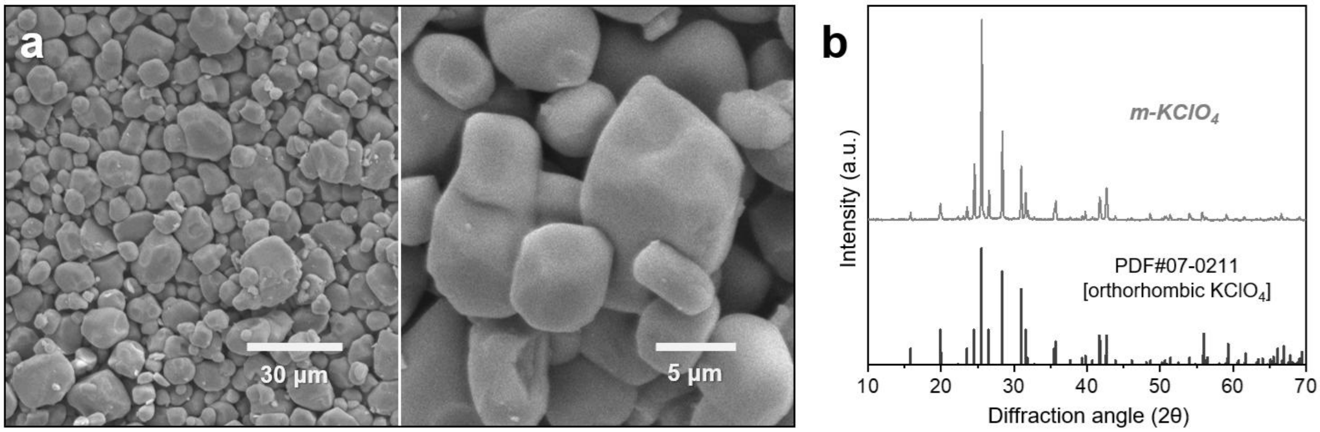

Figure S2. (**a**) *SEM images and* (**b**) *PXRD pattern of micron-sized* $KClO_4$.

○ Note S4. Preparation of binary and ternary composites

All binary and ternary composites, including Al/CF composites in Section 3.2, KP/CF composites in Section 3.3, and Al/KP/CF composites in Section 3.4 and 3.5, were prepared via an ultrasonic dispersion method using isopropyl alcohol (IPA) as dispersion medium. Generally, precise quantities of components were added into 30 mL of IPA in a 50 mL Teflon beaker, and the suspension was homogenized in an ultrasonic bath at 50 °C for 2 h. The obtained mixtures were dried in a vacuum oven at 70 °C for 5 h to remove the residual IPA.

The compositions of binary systems in Section 3.2 and 3.3 can be easily determined, as the content of additive can be an arbitrary value. However, concerning the fuel/oxidizer energetic composites in Section 3.4 and 3.5, their compositions are designed to have an identical fuel-to-oxidizer equivalence ratio (ϕ) defined as follows:

$$\phi = \frac{(m_{fuel}/m_{oxidizer})_{actual}}{(m_{fuel}/m_{oxidizer})_{stoichiometric}}$$

The stoichiometric reactions of Al/$KClO_4$ and Al/CoF_2 under inert atmosphere are expected as follows:

$$Al + \frac{3}{8}KClO_4 = \frac{1}{2}Al_2O_3 + \frac{3}{8}KCl$$

$$Al + \frac{3}{2}CoF_2 = AlF_3 + \frac{3}{2}Co$$

In this work, all Al/KP/CF energetic composites (see **Table S2**) were designed to have an identical equivalence ratio of **ϕ=1.3**, which means that 1.3 mol of active Al is coupled with 0.375 mol of $KClO_4$ or 1.5 mol of CoF_2. In other words, 100 mg of m-Al powder (63 mg active Al) is coupled with 93.92 mg of $KClO_4$ or 261.14 mg of CoF_2.

Table S2. *Composition of energetic composites based on m-Al, $KClO_4$, and p-CoF_2.*

Sample label	Mass fraction of component [%]			Mass fraction of composite [%]	
	ω(Al)	ω($KClO_4$)	ω(CoF_2)	ω(Al/KP)	ω(Al/CF)
Al/KP	51.7	48.3	0	100	0
Al/KP/$CF_{5\%}$	50.1	44.9	5	93.1	6.9
Al/KP/$CF_{10\%}$	48.4	41.6	10	86.2	13.8
Al/KP/$CF_{20\%}$	45.1	34.9	20	72.3	27.7
Al/KP/$CF_{30\%}$	41.8	28.2	30	58.5	41.5
Al/KP/$CF_{45\%}$	36.8	18.2	45	37.8	62.2
Al/CF	27.7	0	72.3	0	100

Moreover, due to the consistent equivalence ratio, the ternary Al/KP/CF composites can also be regarded as the linear combination of binary Al/KP and Al/CF composite in the form of vector equation as follows:

$$\begin{bmatrix} \omega(Al) \\ \omega(KClO_4) \\ \omega(CoF_2) \end{bmatrix}_{Al/KP/CF} = \omega(Al/KP) \cdot \begin{bmatrix} \omega(Al) \\ \omega(KClO_4) \\ 0 \end{bmatrix}_{Al/KP} + \omega(Al/CF) \cdot \begin{bmatrix} \omega(Al) \\ 0 \\ \omega(CoF_2) \end{bmatrix}_{Al/CF}$$

where

$$\omega(Al)_{Al/KP} = \frac{100}{100 + 93.32} = 51.73\%, \qquad \omega(KClO_4)_{Al/KP} = \frac{93.32}{100 + 93.32} = 48.27\%$$

$$\omega(Al)_{Al/CF} = \frac{100}{100 + 261.14} = 27.69\%, \qquad \omega(CoF_2)_{Al/CF} = \frac{261.14}{100 + 261.14} = 72.31\%$$

● Thermal oxidation of m-Al

○ Note S5. Thermal analysis of bare m-Al in air

Commercial micron-sized aluminum powder (m-Al, 1−2 μm in diameter, **Figure S3**) was purchased from Zhonghangzhongmai metal material Co. Ltd, China. This m-Al powder was utilized in our previous works [3], wherein the data can be referenced for comparison.

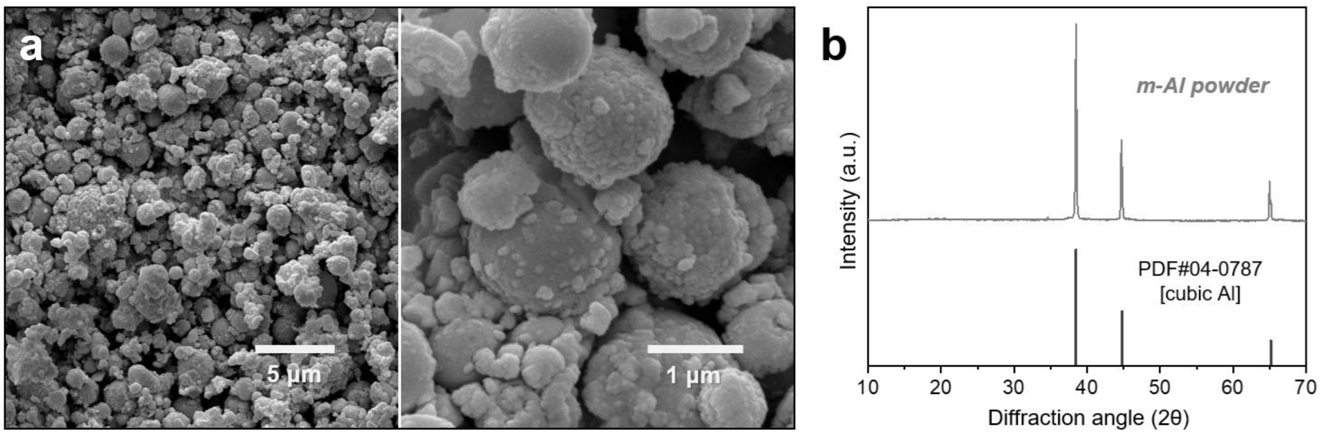

Figure S3. (**a**) *SEM images and* (**b**) *PXRD patterns of m-Al powder.*

Because Al naturally forms an Al_2O_3 passivation layer when exposed to air, commercial Al powder consists of unoxidized Al core and Al_2O_3 passivation shell. Thermogravimetric analysis (TGA) is a common method to quantify the statistical content of unoxidized Al (see **Figure S4**). Since Al_2O_3 is the sole oxidation product of Al under normal conditions, the total percent weight gain (fixation of oxygen from air) after complete oxidation (when the sample mass does not further increase, typically >1100 °C) can be used to calculate the active Al content as follows:

$$2Al_{(s)} + \frac{3}{2}O_{2(g)} \rightarrow Al_2O_{3(s)}$$

$$R_{g,(Al/O)} = \left(\frac{m(Al)}{m(O)}\right)_{Al_2O_3} = \frac{M(Al)}{M(O)} \cdot \left(\frac{n(Al)}{n(O)}\right)_{Al_2O_3} = \frac{26.982}{15.999} \cdot \frac{2}{3} \approx 1.1243$$

$$\omega(active\ Al) = \frac{m(active\ Al)}{m(raw\ Al)} = \frac{R_{g,(Al/O)} \cdot m(solified\ O)}{m(raw\ Al)} = 1.1243 \cdot (\Delta m_{\%})_{oxidation}$$

Furthermore, owing to surface adsorbed water and bound water (in the form of AlO(OH) and $Al(OH)_3$), a minor low-temperature dehydration (complete at 300−500 °C) generally precedes the onset of oxidation. As the dehydration process is independent of the atmosphere, the content of water can be further verified by TGA under an inert atmosphere where only dehydration will occur.

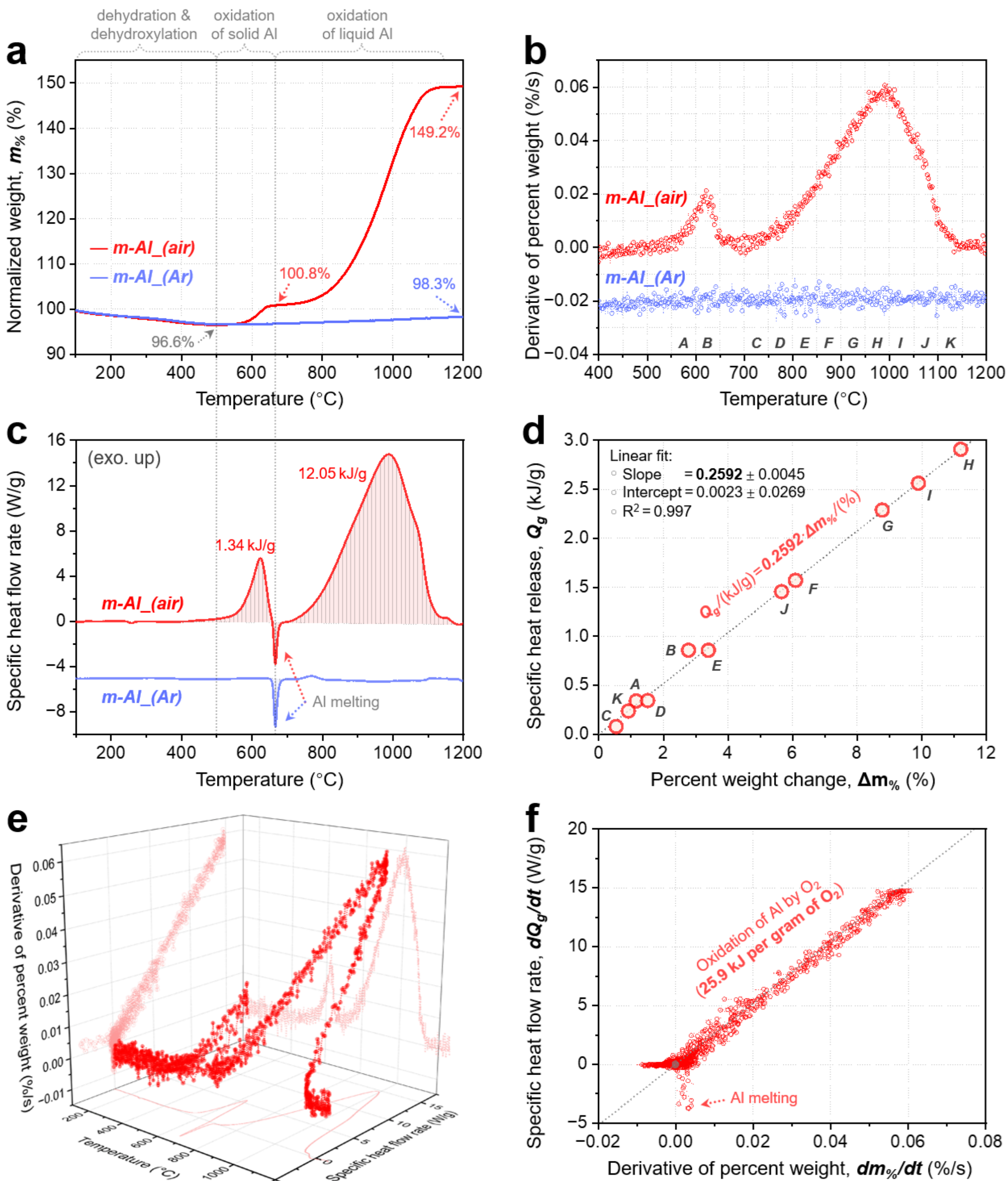

Figure S4. *Thermal analyses of m-Al powder at heating rate of 15 °C·min^{-1}.* (**a**) *TG curves,* (**b**) *DTG curves, and* (**c**) *DSC curves under air and argon atmosphere, respectively.* (**d**) *Correlation between* *specific heat release and percent weight increase of m-Al in air over a series of temperature intervals (Capital letters are associated with those in (b). For example, 'A' represents the temperature interval of 550−600 °C).* (**e**) *Relationship among weight change rate, heat flow rate, and temperature in a 3D plot.* (**f**) *Correlation between specific heat flow rate and percent weight increase rate.*

Notably, the m-Al powder used in this work has an active content of ~63% by mass, significantly lower than that of general Al powder (~80 % active Al). This low active content and thick passivation layer resulted from inappropriate storage (exposed to air for several months and then dehydrated at 250 °C for 1h). Although using intact Al powder with high active content is beneficial for high performance, we intentionally employed this partially degraded m-Al powder. The oxidation of such less reactive Al poses a greater challenge compared to high-quality Al, thereby more effectively demonstrating the superior functionality of CoF_2.

From a methodological perspective, although Al oxidation has been extensively studied via simultaneous TG-DSC, the relationship between the weight change and heat flow is generally addressed in qualitative manners, lacking rigorous quantitative analysis. For oxidation of bare m-Al in air, the DTG curve ($d(m/m_0)/dt$, **Figure S4**b) and DSC curve ($d(Q/m_0)/dt$, **Figure S4**c) showed a marked similarity (except for the Al melting peak), which originates from the stoichiometry of the Al/O_2 reaction ($4Al+3O_2 \rightarrow 2Al_2O_3$). The ratio of heat release to weight increase (i.e., $Q_g/\Delta m_{\%}$, the integral form ratio, **Figure S4**d) is mathematically equivalent to the ratio of heat release rate to weight increase rate (i.e., $(dQ_g/dt)/(dm_{\%}/dt)$, the differential form ratio, **Figure S4**f). Both ratios (25.92 kJ/g) reflected the heat release with unit amount of O_2 gas solidified to Al_2O_3 (i.e., 25.92 kJ per gram of O). Notably, this measured value is lower than the standard enthalpy of 34.91 kJ per gram O (corresponds to 31.05 kJ per gram of Al, see Table SX in Note S6), probably because the produced Al_2O_3 at low temperature is in an amorphous form rather than the thermodynamically stable α-Al_2O_3 (corundum).

It is noteworthy that the $Q/\Delta m$ ratio in the Al/O_2 reaction is independent of factors such as particle size of Al, extent of reaction, active Al content, and the content of non-reactive additive (e.g., Al_2O_3 passivation shell). While this ratio is theoretically temperature-dependent (due to heat capacity differences between reactants and products) and decreases slightly at high temperature, the observed variation was negligible throughout the test.

○ Note S6. Influence of fluoride on Al and Al_2O_3

To determine whether the high-temperature mass loss of p-CoF_2 originates from its own volatilization or other reactions (e.g., reaction with the alumina crucible forming volatile AlF_3), we added n-Al_2O_3 (Shanghai Aladdin Reagent, 20 nm) to p-CoF_2 and compared the thermal behavior of the n-Al_2O_3/p- p-CoF_2 composite (40 wt% n-Al_2O_3) with that of bare n-Al_2O_3 and p-CoF_2 (**Figure S5**). The results show that adding n-Al_2O_3 significantly lowers the temperature range for p-CoF_2 mass loss and eliminates its melting endothermic peak, indicating the occurrence of reaction between p-CoF_2 and Al_2O_3. Furthermore, it is noteworthy that the high-temperature behavior of p-CoF_2 in this work differs slightly from that of our previous results for CoF_2 nanoparticles [4], mainly attributed to the difference on testing sample mass (~5 mg for p-CoF_2 vs. ~11 mg for n-CoF_2).

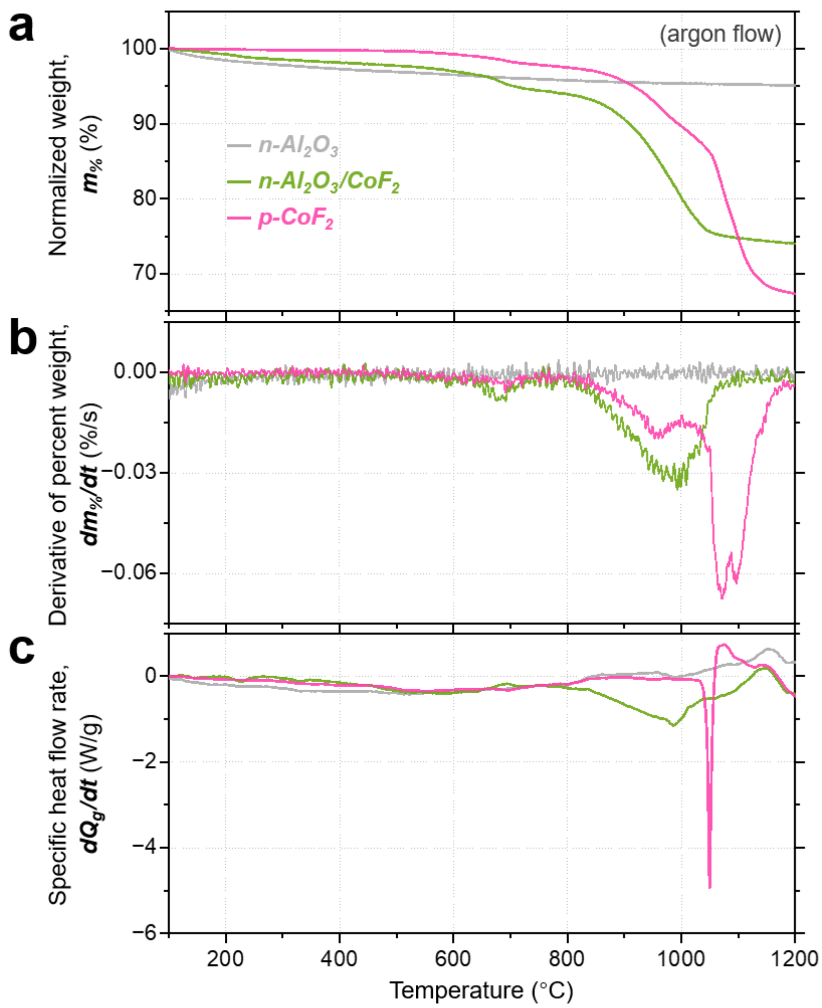

Figure S5. *Thermal analysis of n-Al_2O_3, p-CoF_2, and n-Al_2O_3/p-CoF_2 composite at heating rate of 15 °C·min^{-1} under argon atmosphere.* (**a**) *TG curves,* (**b**) *DTG curves,* (**c**) *DSC curves*.

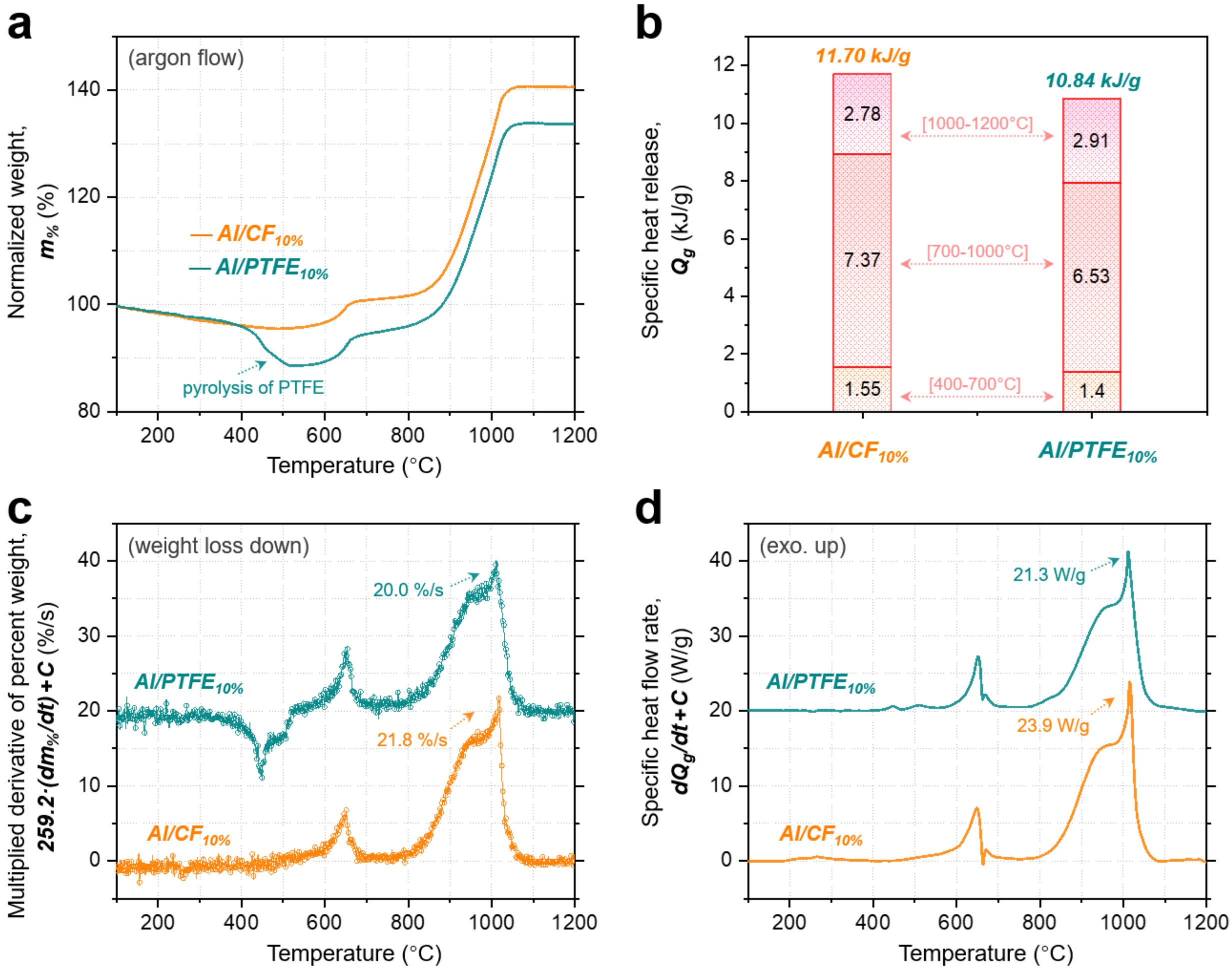

Figure S6. *Comparison of influence between p-CoF_2 and PTFE with same loading of 10 wt.% in m-Al. Thermal analyses are conducted at heating rate of 15 °C·min^{-1} under argon atmosphere.*

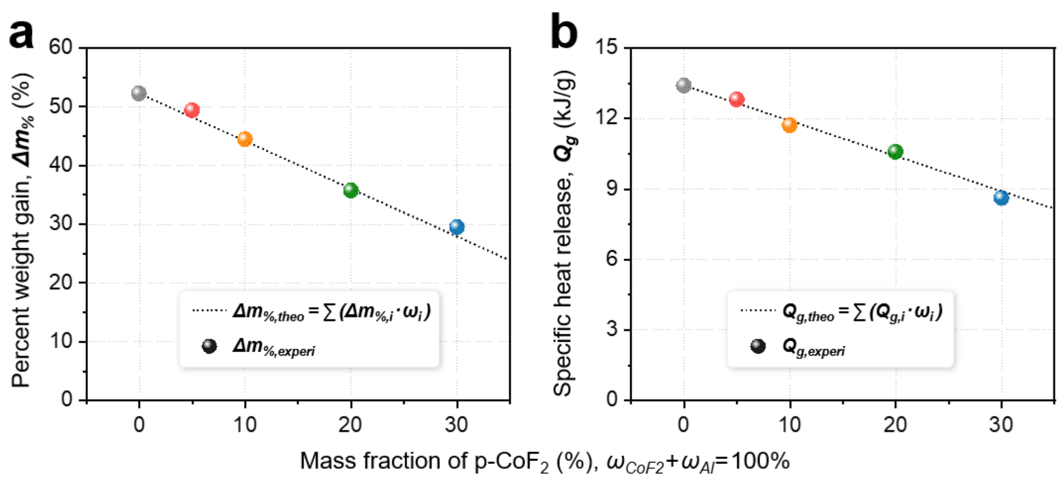

Figure S7. *The influence of p-CoF_2 content on* (**a**) *total weight gain and* (**b**) *total heat release of Al/CF composites*.

Concerning the thermal analysis results in Figure 2 in the main text, the overall weight gain and heat release of Al/CF composites are approximate to the weighted average values of m-Al and p-CoF_2 based on their mass content (**Figure S7**) as follows:

$$\begin{bmatrix} \Delta m_{\%} \\ Q_g \end{bmatrix}_{Al/CF} \approx \omega(mAl) \cdot \begin{bmatrix} \Delta m_{\%} \\ Q_g \end{bmatrix}_{mAl} + \omega(pCoF_2) \cdot \begin{bmatrix} \Delta m_{\%} \\ Q_g \end{bmatrix}_{pCoF_2}$$

where

$$\begin{bmatrix} \Delta m_{\%} \\ Q_g \end{bmatrix}_{mAl} = \begin{bmatrix} +55.2\% \\ +13.4\ kJ/g \end{bmatrix}, \qquad \begin{bmatrix} \Delta m_{\%} \\ Q_g \end{bmatrix}_{pCoF_2} = \begin{bmatrix} -29.0\% \\ -1.6\ kJ/g \end{bmatrix}$$

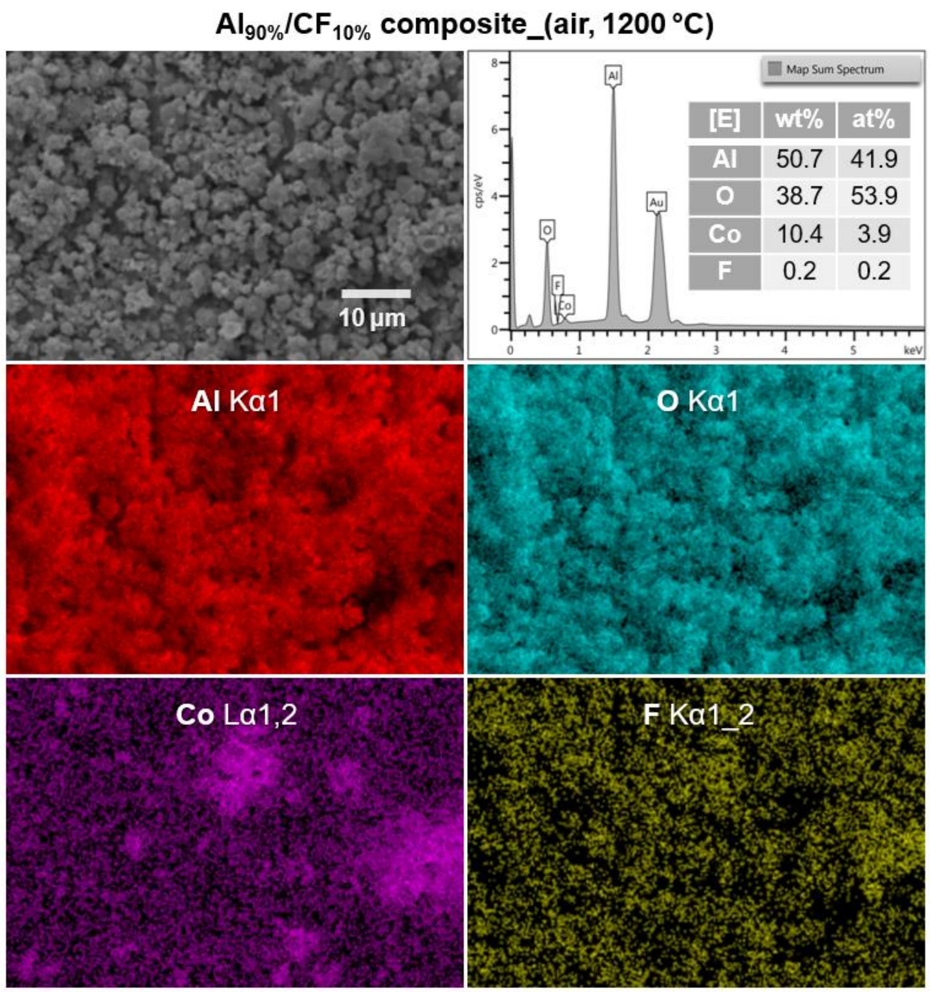

Figure S8. *EDS analysis of residue of Al/$CF_{10\%}$ composite heated up to 1200 °C in air.*

● Catalytic decomposition of $KClO_4$

○ Note S7. Thermal analysis of $KClO_4$/p-Co_3O_4 composites

The thermal decomposition mechanism of $KClO_4$ has been extensively studied [5-7], and the generally accepted reaction pathway is represented as follows:

$$KClO_4 \rightarrow KCl + 2O_2 \uparrow, \qquad \begin{cases} KClO_4 \rightarrow KClO_3 + \frac{1}{2}O_2 \uparrow \\ KClO_3 \rightarrow KCl + \frac{3}{2}O_2 \uparrow \\ \frac{1}{4}KCl + \frac{3}{4}KClO_4 \leftrightarrow KClO_3 \end{cases}$$

To complement Section 3.3, we performed comparative thermal analysis on $KClO_4$/p-Co_3O_4 composites (**Figure S9**).

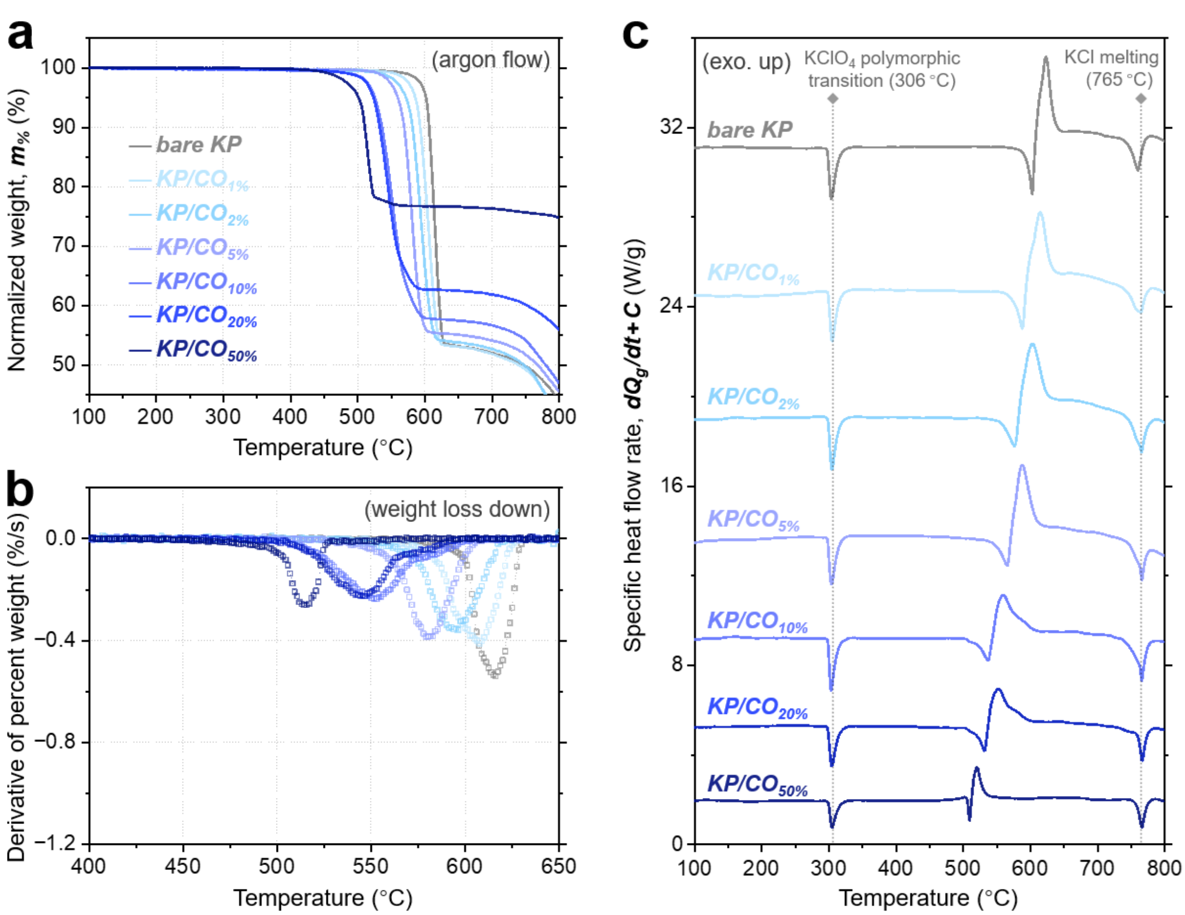

Figure S9. *Thermal analysis of bare $KClO_4$ and $KClO_4$/p-Co_3O_4 composites.* (**a**) *TG curves,* (**b**) *DTG curves,* (**c**) *DSC curves at heating rate of 15 °C·min^{-1} under argon atmosphere.*

Notably, it is necessary to clarify regarding the terms 'catalyst' and 'catalyze'. Although a catalyst is conventionally defined as an additive that alters the reaction pathway without being consumed by the reaction, the term 'combustion catalyst' is widely used in the field of energetic materials to broadly refer to the substances that can modify the decomposition behaviors of oxidizers and explosives. Since energetic materials are inherently disposable, researchers in this field primarily focus on materials' ability to alter decomposition behavior rather than their recoverability after the reaction. Therefore, some so-called 'combustion catalysts' may not meet the traditional definition of catalysts. In this work, while both CoF_2 and Co_3O_4 act as combustion catalysts for $KClO_4$ decomposition, only Co_3O_4 qualifies as a true catalyst. Nevertheless, we believe that the use of 'catalyst' and 'catalyze' here will not cause significant conceptual ambiguity.

○ Note S8. Non-isothermal kinetic analysis

Non-isothermal kinetic analysis based on TG-DTG-DSC data can provide important insights into the fundamental issues of the stability and reactivity of materials. According to the Arrhenius equation, the reaction rate constant k can be described as a function of temperature T (in Kelvin) as follows:

$$k = A \cdot \exp\left(-\frac{E_a}{R \cdot T}\right)$$

where A is the pre-exponential factor, E_a is the activation energy, and R is the gas constant (8.314 $J \cdot K^{-1} \cdot mol^{-1}$). Among several non-isothermal analytical methods developed based on the Arrhenius equation, the Kissinger method is one of the most commonly used approaches for determining the apparent activation energy (E_a) [8, 9], based on the peak temperatures at multiple heating rates as follows:

$$\ln\left(\frac{{T_p}^2}{\beta}\right) = E_a \cdot \frac{1}{R \cdot T_p} + C$$

where T_p is the peak temperature of DTG or DSC curves (the temperature for the maximum reaction rate), β (in units of $K \cdot min^{-1}$ or $°C \cdot min^{-1}$) is the heating rate, and C is a constant. Accordingly, the apparent activation energy E_a can be calculated from the slope of the regression line obtained from plotting $\ln({T_p}^2/\beta)$ against $1/T_p$.

The DTG and DSC peak temperatures corresponding to $KClO_4$ decomposition are listed in **Table S3** (corresponding to the data in Figure 3g in main text).

Table S3. *Peak temperatures of $KClO_4$ decomposition in DTG and DSC curves at various heating rates*.

Heading rate [K·min^{-1}]	bare KP		$KP/CF_{5\%}$		$KP/CO_{5\%}$	
	$T_{p,DTG}$ [K]	$T_{p,DSC}$ [K]	$T_{p,DTG}$ [K]	$T_{p,DSC}$ [K]	$T_{p,DTG}$ [K]	$T_{p,DSC}$ [K]
5	596.53	601.45	500.95	502.01	556.32	557.51
10	607.30	614.39	503.92	506.01	569.67	573.41
15	615.95	623.20	506.26	511.50	582.05	587.80
20	621.58	629.37	507.81	514.73	590.04	595.79
25	628.83	641.51	509.70	516.15	597.38	603.31

Despite the simplicity of conventional Kissinger method, it assumes constant activation energy during the reaction, yielding oversimplified or inaccurate kinetic parameters, especially in the analysis of overlapped multi-step reactions. To resolve this limitation, isoconversional methods like Kissinger-Akahira-Sunose (KAS) method can be employed. KAS method analyzes kinetic parameters at fixed degree of conversion (based on mass change or heat effect) [10, 11], providing conversion-dependent activation energy as follows:

$$\ln\left(\frac{{T_\alpha}^2}{\beta}\right) = E_\alpha \cdot \frac{1}{R \cdot T_\alpha} + C, \qquad \alpha = \frac{m_{initial} - m(T_\alpha)}{m_{initial} - m_{final}}$$

where the degree of conversion (α) is based on the mass change during decomposition, T_α is temperature corresponding to certain degree of conversion and E_α is the corresponding isoconversional activation energy.

The results of thermal analysis at various heating rates are shown in **Figure S10** (corresponding to the data in Figure 3f in main text).

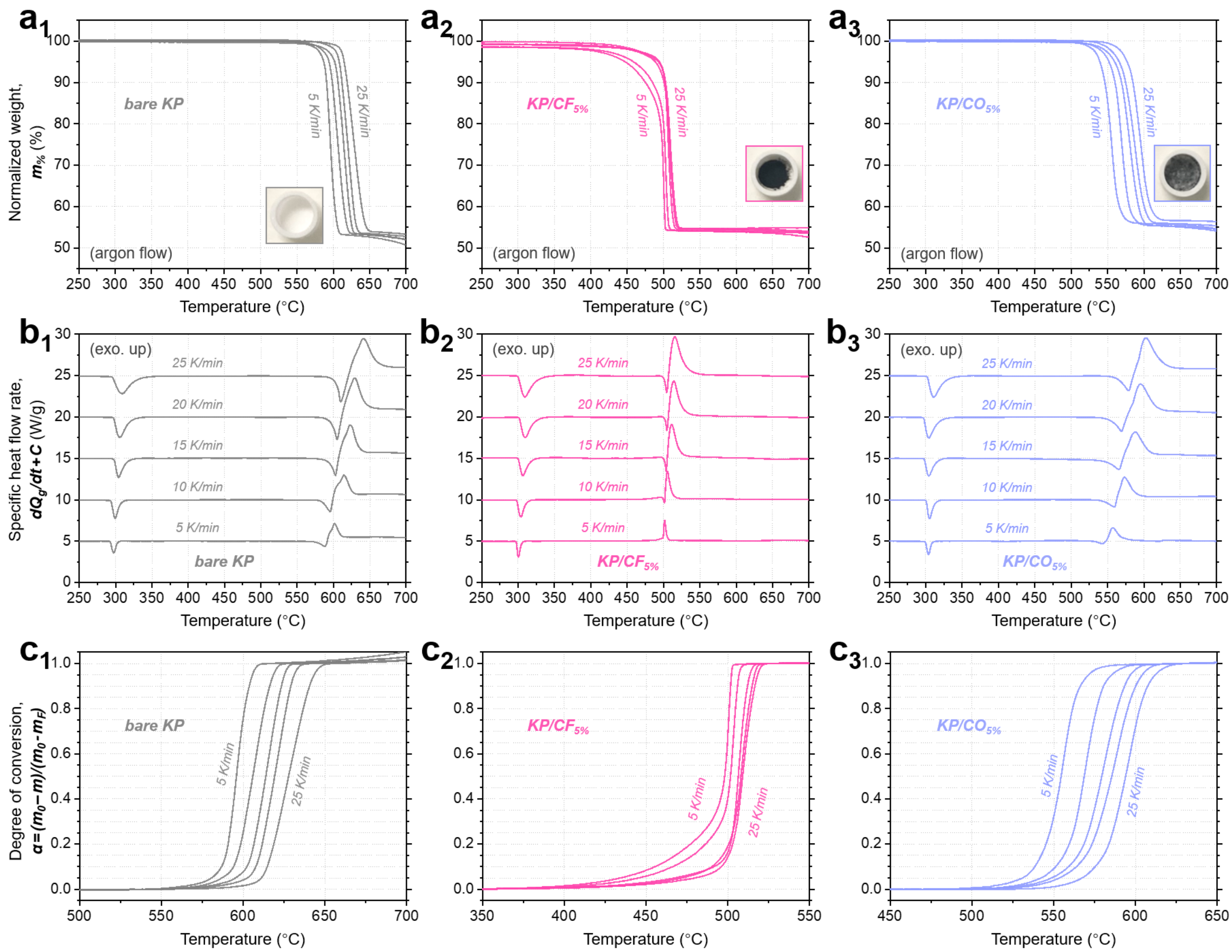

Figure S10. *Thermal analysis of bare $KClO_4$, KP/CF$_{5\%}$, and KP/CO$_{5\%}$ at various heating rates (5, 10, 15, 20, and 25 °C·min^{-1}) under argon atmosphere.* **(a)** *TG curves,* **(b)** *DTG curves,* **(c)** *Degree of conversion based on weight change. The inset photos in (a_{1-3}) shows the residues after tests.*

● Reactive performance of energetic composites

○ Note S9. Reaction efficiency

Since all energetic composites in Section 3.4 and 3.5 in main text are fuel-rich (see Table S2), their theoretical heat releases of composites can be calculated based on complete consumption of oxidizer as follows:

$$Q_{g,Al/KP} = \omega(KClO_4)\cdot\frac{M(Al)+0.375\cdot M(KClO_4)}{0.375\cdot M(KClO_4)}\cdot Q_g{}^{\circ}{}_{(Al/KClO_4)} = 73.4\%\cdot 10.63\ kJ/g = 7.80\ kJ\cdot g^{-1}$$

$$Q_{g,Al/CF} = \omega(CoF_2)\cdot\frac{M(Al)+1.5\cdot M(CoF_2)}{1.5\cdot M(CoF_2)}\cdot Q_g{}^{\circ}{}_{(Al/CoF_2)} = 85.7\%\cdot 2.74\ kJ/g = 2.35\ kJ\cdot g^{-1}$$

$$Q_{g,Al/KP/CF} = \omega(Al/KP)\cdot Q_{g,Al/KP} + \omega(Al/CF)\cdot Q_{g,Al/CF}$$

The theoretical heat releases of stoichiometric reaction (***Q**$_g$°*) are given in Note S15 in this file. The reaction efficiency (η) is defined as the ratio of experimental heat releases to theoretical heat releases.

Table S4. *Experimental and theoretical heat releases of Al/KP/CF composites.*

Sample label	$Q_{g\ (280\sim550\ °C)}$ [kJ·g^{-1}]	$Q_{g,\ (total)}$ [kJ·g^{-1}]	$Q_g°_{,\ (theo)}$ [kJ·g^{-1}]	Reaction efficiency, η [%]
Al/KP	0.10	0.14	7.8	1.79
Al/KP/CF$_{5\%}$	0.28	0.35	7.42	4.72
Al/KP/CF$_{10\%}$	2.36	2.84	7.05	40.3
Al/KP/CF$_{20\%}$	3.18	3.57	6.29	56.8
Al/KP/CF$_{30\%}$	2.98	3.43	5.54	61.9
Al/KP/CF$_{45\%}$	2.41	2.77	4.41	62.8
Al/CF	0.01	1.78	2.35	75.7

○ **Note S10. Post-characterization**

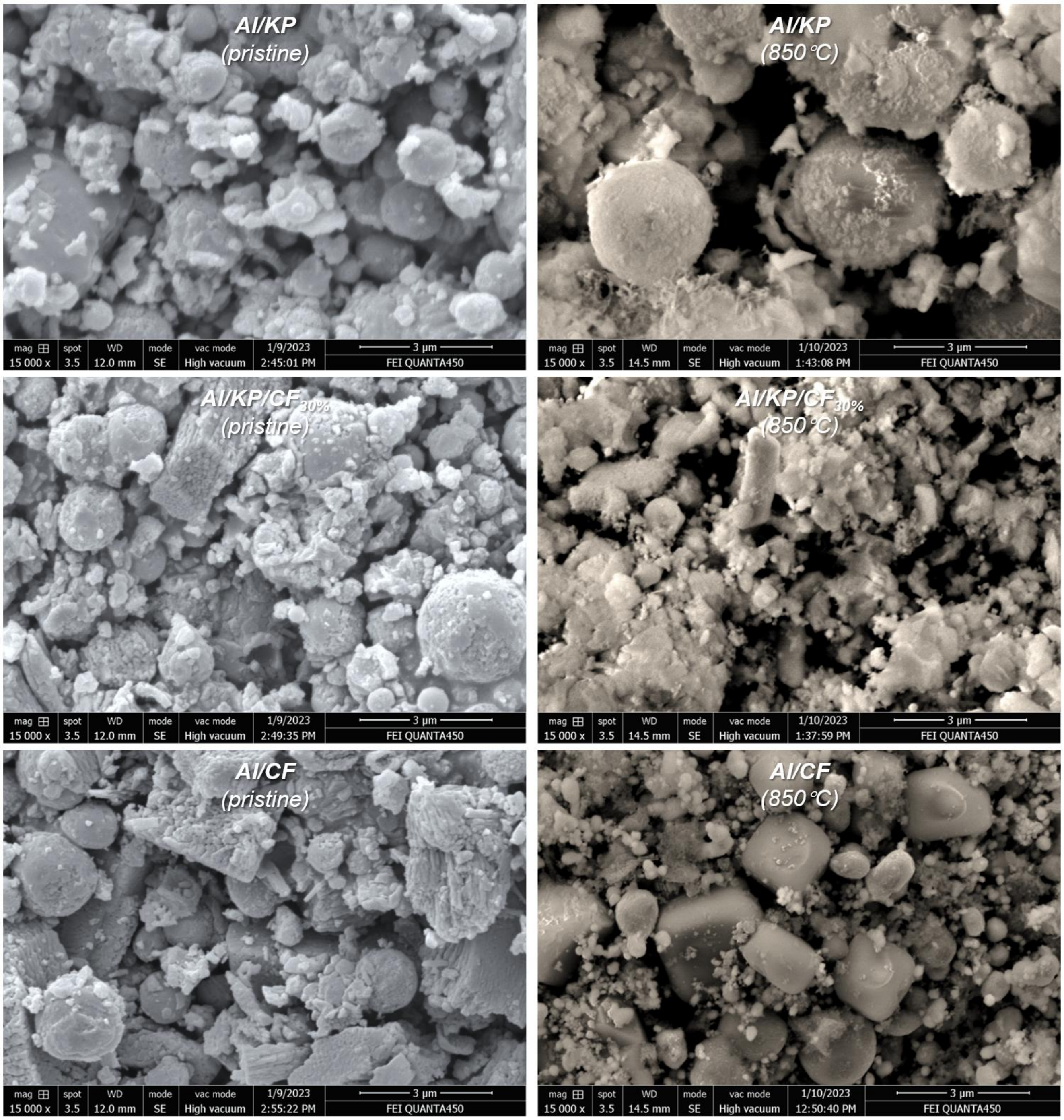

Figure S11. *SEM images of pristine Al/KP/CF composites and reaction products after heating under argon atmosphere up to 850 °C.*

$Al_{27.7\%}/CF_{72.3\%}$ composite_(argon, 850 °C)

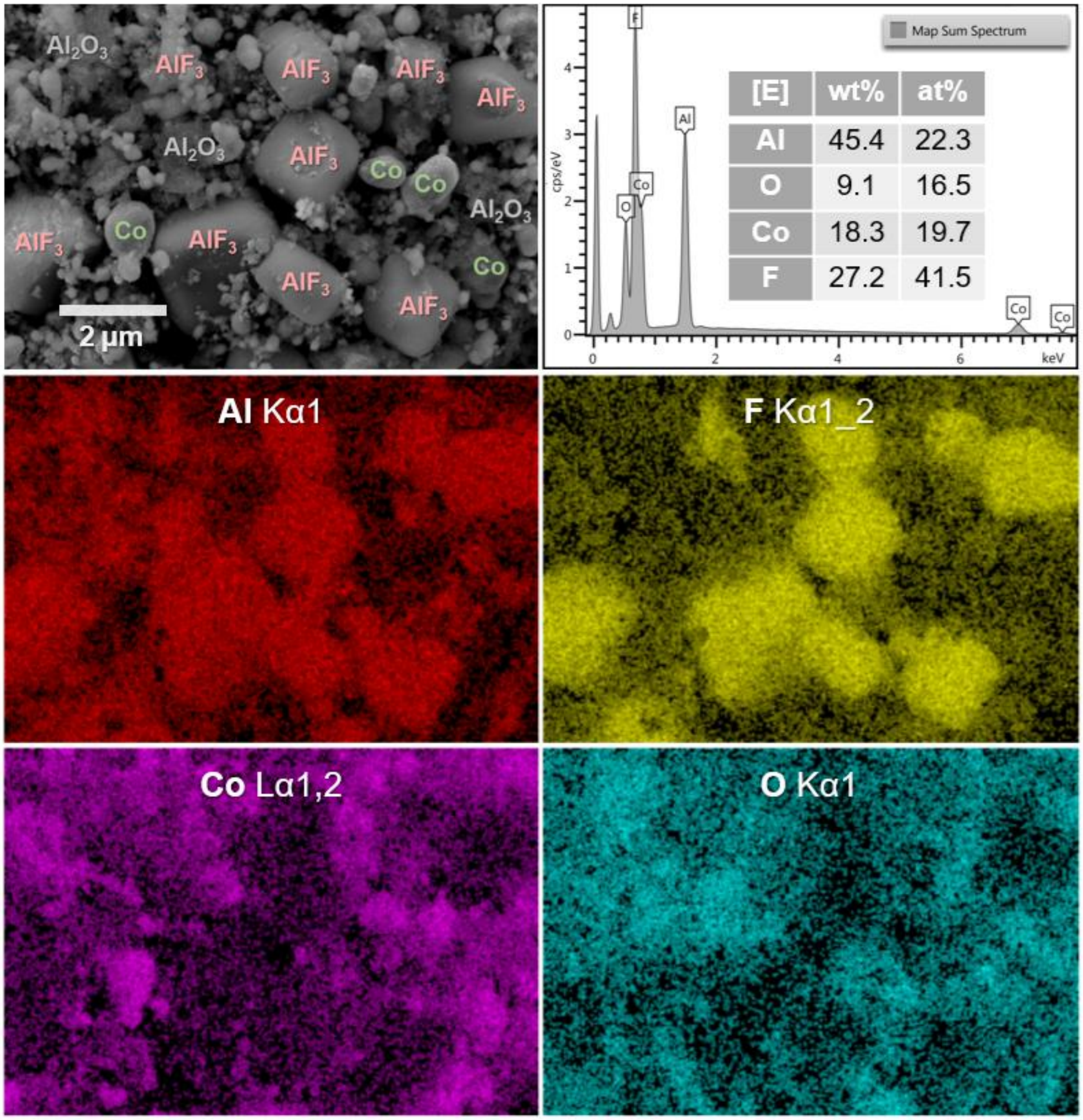

Figure S12. *EDS analysis of residue of Al/CF composite after thermal analysis (corresponds to Al/CF_850 °C in Figure S11).*

○ Note S11. Comparative experiments

The Al/KP/CO$_{30\%}$ composite in Figure S13 is prepared by replacing p-CoF_2 in Al/KP/CF$_{30\%}$ with an equivalent amount of p-Co_3O_4. The nanosized Al powder (n-Al) used for comparative study is the same as those in our previous works [3, 4, 12] (shown in Figure 4g in main text). The n-Al/$KClO_4$ composite in Figure S13 has a n-Al content of 55.8 wt.%.

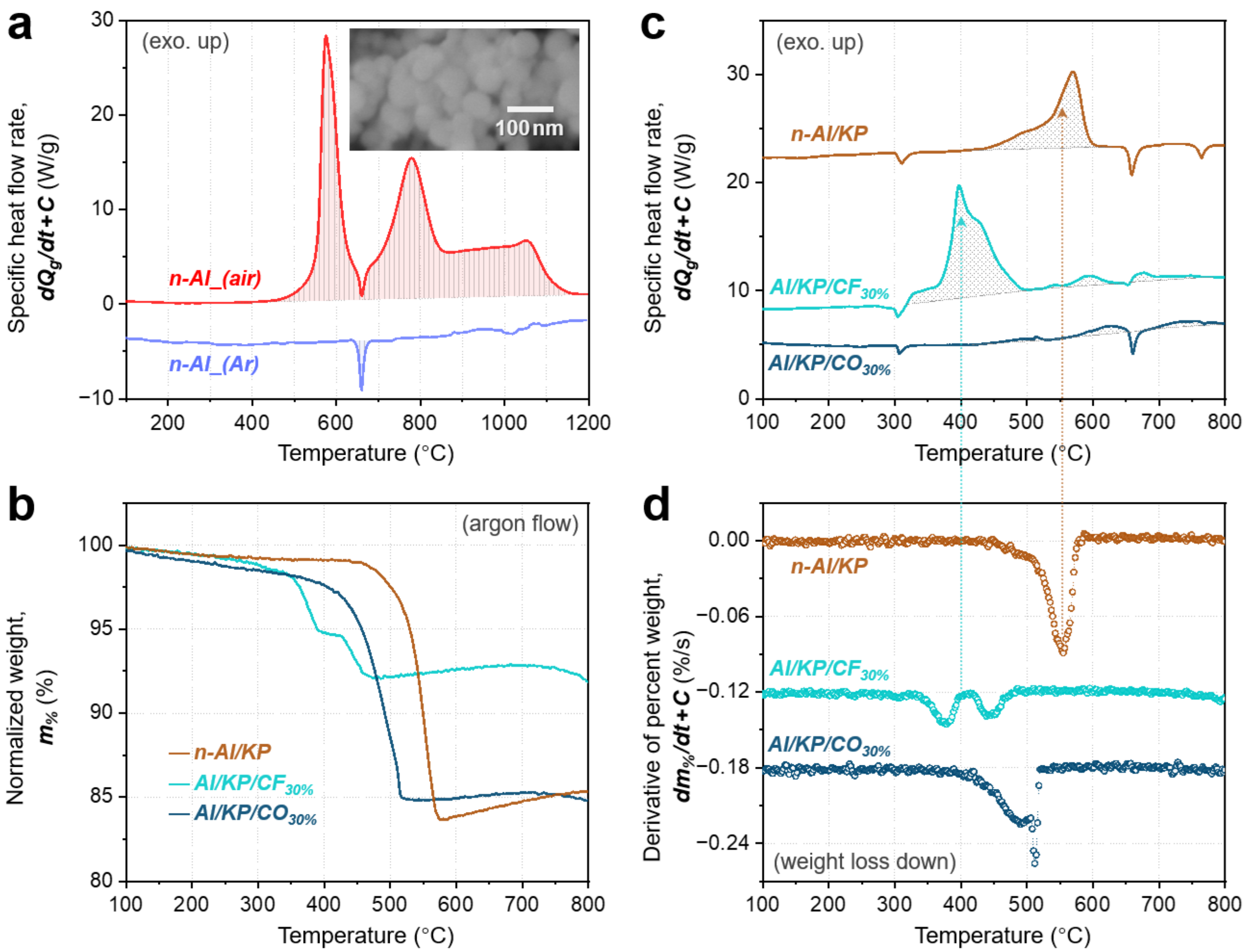

Figure S13. (**a**) *SEM image and DSC curves of nanosized Al under air and argon atmosphere. Thermal analysis of n-Al/$KClO_4$ and m-Al/$KClO_4$/p-Co_3O_4 (Al/KP/CO$_{30\%}$) for comparison study.* (**b**) *TG curves,* (**c**) *DSC curves, and* (**d**) *DTG curves at heating rate of 15 °C·min^{-1} under argon atmosphere.*

○ **Note S12. Long-term compatibility test**

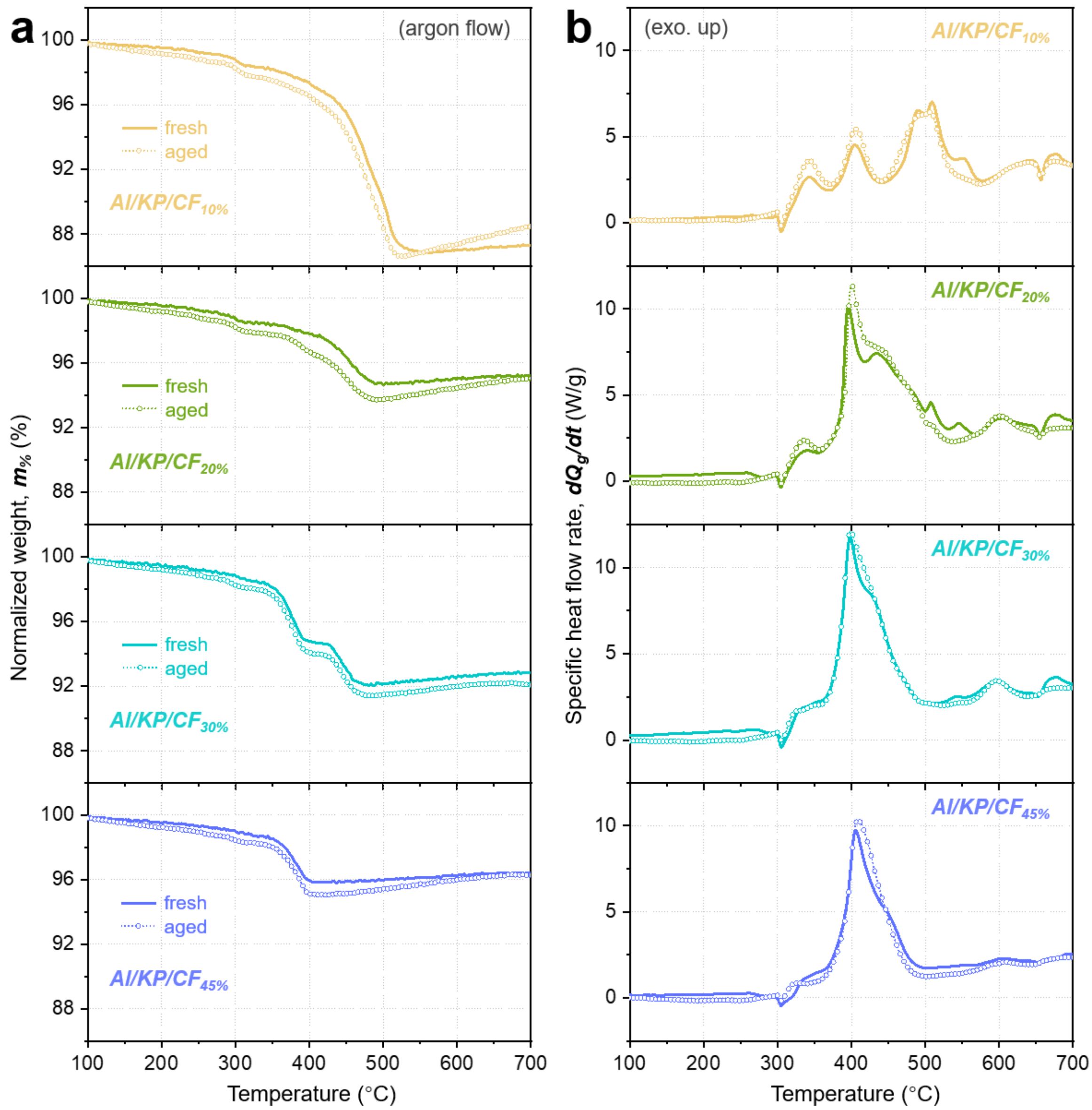

Figure S14. *Comparison between freshly prepared composites and aged composites after 18-month storage at 25 °C, 40% relative humidity.* (**a**) *TG curves and* (**b**) *DSC curves at heating rate of 15 °C·min^{-1} under argon atmosphere*.

● Combustion test

○ Note S13. Estimation of heating rate in hotwire ignition

The ignition of energetic composites in combustion tests is achieved through Joule heating of NiCr hotwire at constant current of 3 A. To estimate the heating rate (β=$\Delta T/\Delta t$) under this condition, we conducted a simplified analysis based on energy conversion. Ignoring the heat lost to the environment (adiabatic condition), the input electrical energy is entirely converted into the thermal energy of the hotwire. So, the energy balance can be expressed as follows:

$$\begin{cases} E_{input} = P \cdot \Delta t = I^2 \cdot R \cdot \Delta t = I^2 \cdot \left(\rho_R \cdot l \cdot A^{-1}\right) \cdot \Delta t \\ E_{output} = Q = c_p \cdot m \cdot \Delta T = c_p \cdot \left(\rho_D \cdot l \cdot A\right) \cdot \Delta T \\ E_{input} \approx E_{output} \end{cases}$$

where $\boldsymbol{I}$ is electric current (3 A), $\boldsymbol{\rho_R}$ is electrical resistivity of NiCr ($1.2 \cdot 10^{-6}$ Ω·m), l is wire length, $\boldsymbol{A}$ is cross-sectional area of wire (for diameter of 0.2 mm, $A \approx 3.14 \cdot 10^{-8}$ m^2), $\boldsymbol{c_P}$ is specific heat capacity of NiCr (0.45 J·g^{-1}·K^{-1}), $\boldsymbol{\rho_D}$ is density of NiCr ($8.3 \cdot 10^6$ g·m^{-3}). For conversion of unit, noted that 1 A^2·Ω=1 J·s^{-1}. Using the parameters above, the heating rate can be derived as follow:

$$\beta = \frac{\Delta T}{\Delta t} \approx \frac{I^2 \cdot \rho_R \cdot l \cdot A^{-1}}{c_p \cdot \rho_D \cdot A \cdot l} = \frac{I^2 \cdot \rho_R}{c_p \cdot \rho_D \cdot A^2} \approx \frac{1.08 \cdot 10^{-5}\ [A^2 \cdot \Omega \cdot m]}{3.68 \cdot 10^{-9}\ [J \cdot K^{-1} \cdot m]} \approx 2.9 \cdot 10^3\ [K \cdot s^{-1}]$$

In this case, the heating rate depends on electric current, physical properties of wire materials, and wire diameter. On the other hand, the wire can remain stable at current of 3A, while exceeding this current cause rapid fusing. Therefore, actual temperature of hotwire at 3A should be close to the melting point of NiCr (~1400 °C). Taking it as 1200 °C for instance, the heating duration is approximately 0.4 s.

○ **Note S14. Enlarged frames of burning**

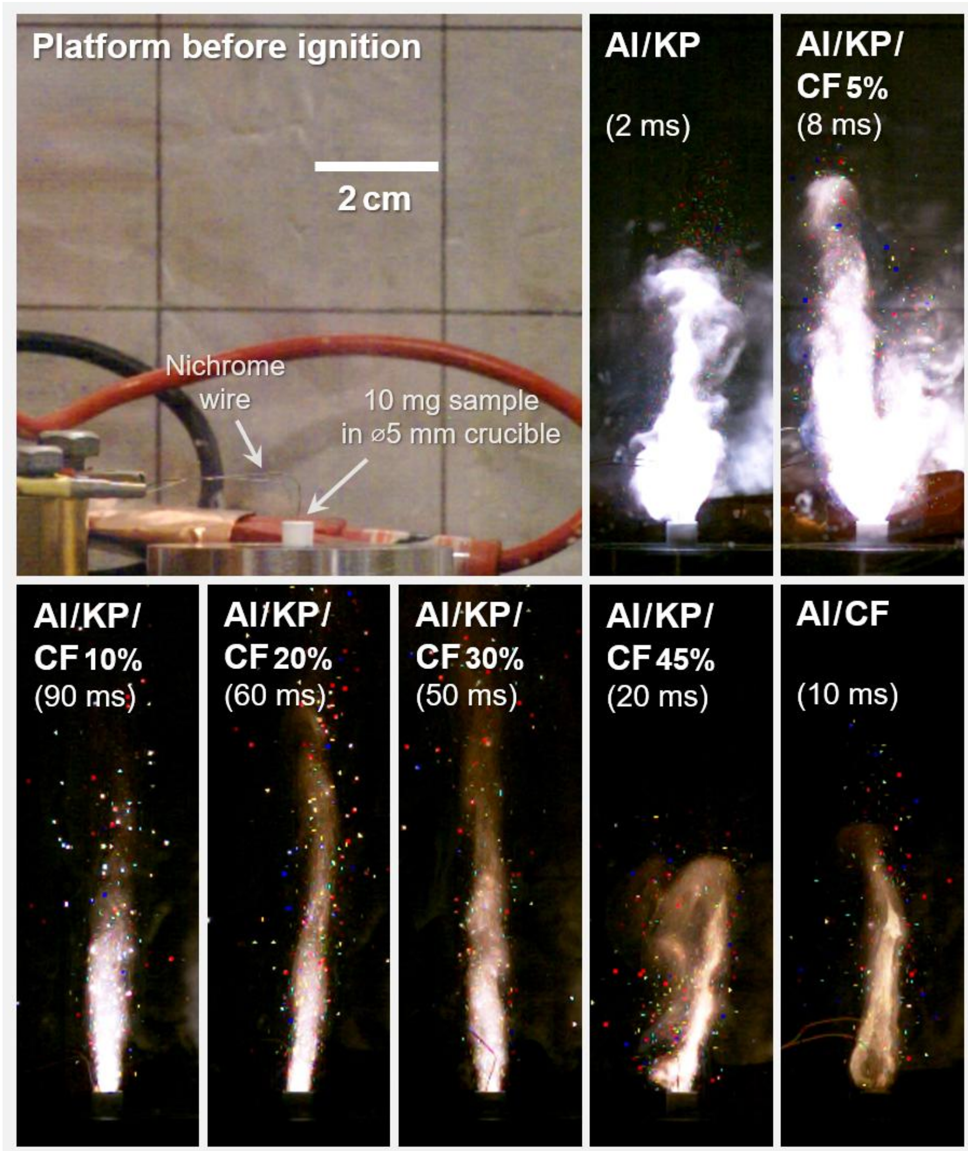

Figure S15. *Photo of open combustion platform and enlarged frames of sample burning at certain times*.

● Physical and thermochemical data

Table S5. *Physical and thermochemical data from Lange's Handbook of Chemistry (17th edition, McGraw Hill, 2016).*

Substance	(state)	Atomic/molecular weight, $\boldsymbol{M}$ [g·mol^{-1}]	Melting point [°C]	Boiling point [°C]	Standard enthalpy of formation, $\boldsymbol{\Delta_f H°}$ [kJ·mol^{-1}]
Al	(s)	26.98	660	2518	0
Al_2O_3	(s)	101.96	2054	2980	−1675.7
AlF_3	(s)	83.98	1090	1272 Subl	−1510.4
Co	(s)	58.93	1492	2900	0
CoF_2	(s)	96.93	1127	1400	−692
Co_3O_4	(s)	240.80	900 dec	-	−891
KCl	(s)	74.55	771	1437	−436.5
$KClO_3$	(s)	122.55	400 dec	-	−397.73
$KClO_4$	(s)	138.55	400 dec	-	−432.8

○ Note S15. Calculation of theoretical heat of reaction

The standard enthalpy of reaction ($\Delta_r H°$) can be calculated from standard enthalpy of formation ($\Delta_f H°$, listed in **Table S5**) based on Hess' law of constant heat summation as follows:

$$v_1 \cdot R_1 + v_2 \cdot R_2 + \cdots \longrightarrow u_1 \cdot P_1 + u_2 \cdot P_2 + \cdots$$

$$\Delta_r H° = \sum_i (u_i \cdot \Delta_f H°(P_i)) - \sum_i (v_i \cdot \Delta_f H°(R_i))$$

It is noteworthy to mention that the value of standard enthalpy of reaction is not a constant but a variable that depends on how the reaction formula is expressed (mole number of reactants involved). On the other hand, theoretical specific heat release can be calculated from the negative standard enthalpy of reaction divided by molar mass of the reactants as follows:

$$Q_g° = \frac{-\Delta_r H°}{\sum_i (v_i \cdot M_i)_{reactant}}$$

Notably, the theoretical heat release is the characteristic value of a certain reaction. The enthalpy and specific heat release of reactions discussed in this work are summarized in **Table S6**.

Table S6. *Standard enthalpy of reaction and corresponding specific heat release*.

No.	Reaction	Enthalpy of reaction $\Delta_r H°$ [kJ·mol^{-1}]	Specific heat release $Q_g°$ [kJ·g^{-1}]
1	$Al + \frac{3}{4}O_2 = \frac{1}{2}Al_2O_3$	−837.9	+31.05 (based on Al) +34.91 (based on O_2) +16.44 (based on Al+O_2)
2	$Al + \frac{3}{2}CoF_2 = AlF_3 + \frac{3}{2}Co$	−472.4	+2.74
3	$\frac{1}{2}Al_2O_3 + \frac{3}{2}CoF_2 = AlF_3 + \frac{3}{2}CoO$	+8.9	+0.304
4	$KClO_4 = KCl + 2O_2$	−3.7	+0.027
5	$Al + \frac{3}{8}KClO_4 = \frac{1}{2}Al_2O_3 + \frac{3}{8}KCl$	−839.2	+10.63

Reference

1. Y. Chen, S. Yang, X. Chen, Y. C. Zheng, Y. Hou, Y. H. Li, H. D. Zeng and H. G. Yang, *Journal of Materials Chemistry A*, 2015, **3**, 15854-15857.
2. B. Zhang, F. Guo, L. Yang, X. Jia, B. Liu, Z. Xie, D. Chen, H. Lu, R. Zhang and Y. Zheng, *Journal of Crystal Growth*, 2017, **459**, 167-172.
3. Y. Li and K. Zhang, *Fuel*, 2025, **383**.
4. Y. Li, K. Meng, M. Tian, L. Zhang, X. Ma and K. Zhang, *Combustion and Flame*, 2024, **265**.
5. A. Simchen, *The Journal of Physical Chemistry*, 1961, **65**, 1093-1096.
6. W. K. Rudloff and E. S. Freeman, *The Journal of Physical Chemistry*, 1969, **73**, 1209-1215.
7. W. K. Rudloff and E. S. Freeman, *The Journal of Physical Chemistry*, 1970, **74**, 3317-3324.
8. H. E. Kissinger, *J. Res. Natl. Bur. Stand*, 1956, **57**, 217-221.
9. H. E. Kissinger, *Analytical chemistry*, 1957, **29**, 1702-1706.
10. S. Vyazovkin, *Thermochimica Acta*, 2024, **733**, 179701.
11. T. Akahira and T. Sunose, *Res Rep Chiba Inst Technol (Sci Technol)*, 1971, **16**, 22-31.
12. Y. Li, I. Hussain, X. Chen, L. Zhang, R. Han, X. Ma and K. Zhang, *ACS Applied Nano Materials*, 2023, **6**, 12219-12230.